Teleseismic interferometry in studying shallow subsurface structures: Detection of interfaces beneath Antarctic stations

Thanh-Son Pham[1], Hrvoje Tkalčić[2], Brian L. N. Kennett[3] and Malcolm Sambridge[4]

1. Corresponding Author. PhD Student, Research School of Earth Sciences, The Australian National University, Canberra ACT 2601, Australia. Email: ThanhSon.Pham@anu.edu.au.

2. Associate Professor, Research School of Earth Sciences, The Australian National University, Canberra ACT 2601, Australia. Email: Hrvoje.Tkalcic@anu.edu.au.

3. Professor, Research School of Earth Sciences, The Australian National University, Canberra ACT 2601, Australia. Email: Brian.Kennett@anu.edu.au.

4. Professor, Research School of Earth Sciences, The Australian National University, Canberra ACT 2601, Australia. Email: Malcolm.Sambrigde@anu.edu.au.

Abstract

Teleseismic waves that propagate near-vertically beneath seismic receivers, reflect from the free surface, propagate downwards and are subsequently reflected again back to the surface. Thus a single station can be used to convert a time series to a reflectivity record by means of computing autocorrelation. For Antarctic stations deployed on ice, most teleseismic energy is trapped between the sharp impedance jump at the ice-rock interface and the free surface. Due to the pronounced reverberations, we observe clear reflections from the interface and their multiples on both vertical and radial autocorrelograms. Picked reflection times are used to estimate the ice thickness by means of seismic velocity that can be obtained from glaciological studies, and v_p/v_s ratio. Our estimates at a pilot station show a good agreement with prior knowledge of the Antarctic ice cap. We also show a synthetic test to confirm our interpretation.

Keywords: computational seismology, seismic interferometry, glaciology.

INTRODUCTION

A thick permanent glacier, whose thickness reaches up to approximately 4.5 km in some places, covers the vast majority of Antarctica [*Fretwell et al.*, 2013]. So far, most thickness measurements of the Antarctic ice cap have been obtained via airborne radar sounding, over-snow radar or seismic sounding, all active source type of studies. The thickness dataset was compiled into a regularly gridded form as a part of the Bedmap project [*Lythe et al.*, 2001] and recently improved Bedmap2 [*Fretwell et al.*, 2013]. Although the data cover the entire continent, their precision is not of a uniform quality due to the limited coverage of measurement campaigns. In this study, we present a possible alternative tool to the existing methods in order to obtain the ice thickness and v_p/v_s measurements by passive seismological data. This might help to complement the databases where their resolution is poor. Previously, this problem was approached by *Hansen et al.* (2010) in their seismological study covering Eastern Antarctica; they inverted for the ice thickness from P-wave receiver functions.

Our aim is to convert both vertical and radial seismogram segments containing the first P arrival and its reflection and conversion (the P-wave coda) [e.g. *Rondenay*, 2009], into an easy-to-interpret form by means of computing autocorrelations. From there, one is able to obtain good estimates of either P, S or both wave travel times in a nearly vertical direction, which can be used to estimate the ice thickness. This is possible because average seismic velocities of the Antarctic ice cap are known from other glaciological studies [e.g. *Kohnen*, 1974]. Similar ideas have been recently used by *Ruigrok and Wapenaar* (2012) and *Sun and Kennett* (2016) to study crustal properties in Tibet and Australia, respectively.

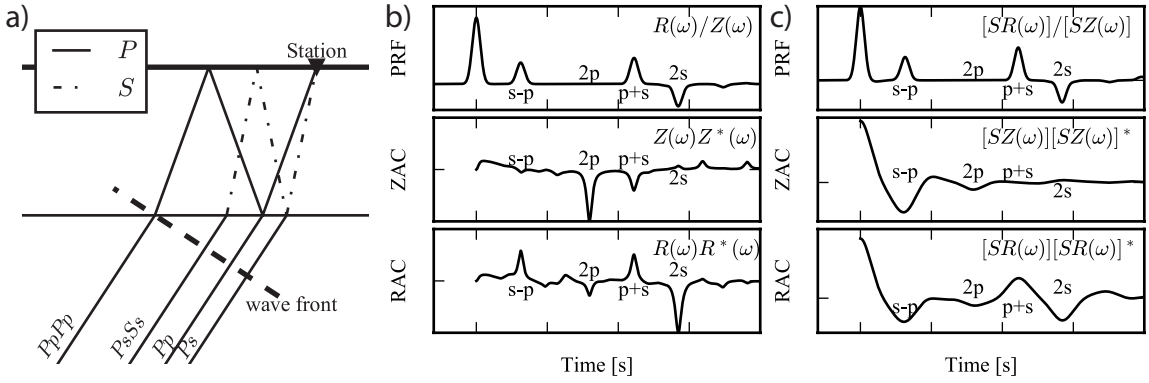

Figure 1 (a) A simple structural configuration of a homogeneous ice layer sitting on top of a half space crustal rock. A plane P wavefront (thick dash line) approaches the layer from below. (b) Comparison of (from top to down): P-wave receiver function (PRF), vertical autocorrelogram (ZAC), and horizontal autocorrelogram (RAC) of the configuration sketched in (a) for the source time defined as an impulse function. These autocorrelograms are tapered to suppress the characteristic peak at time 0. (c) Same as (b) but horizontal and vertical components are convolved with a synthetic seismogram containing both source and intermediate path effect.

To facilitate the interpretation of the autocorrelograms we consider a simple configuration sketched in Figure 1a. A station sitting on top of a homogeneous ice layer and a half space of crustal rock records an impulsive P wave plane arriving nearly vertically. Hence, ground motion records comprise impulsive peaks at different time delays. One can observe the first and strongest peak of the direct ray *Pp*, followed by the converted *Ps* and the single reflection *PpPp*. Any couple of peaks on the original record collapses into a single peak on the autocorrelogram. For instance, the most prominent peak in the vertical autocorrelogram, denoted as 2p (see Figure 1b), is the cumulative contribution of couples having the same relative distance as *Pp* and *PpPp*, and its offset is given by:

$$\Delta t = t_{PpPp} - t_{Pp} = 2H\sqrt{\frac{1}{v^2} - p^2} = 2H\eta, \quad (1)$$

where H is the thickness, v is the P wave velocity, p is the ray parameter and η is the vertical slowness of the plane wave. We refer to [*Zhu and Kanamori*, 2000] for a similar derivation. Similarly, the 2s peak on the horizontal autocorrelogram (Figure 2b) is the cumulative contribution of all phase couples having the same relative distance as *PsSs* and *Ps* and its offset is also given by (1) but v in this case stands for S wave velocity. The same arguments apply for the formation of other peaks.

The seismic wavefield is induced by the source and subsequently modulated and attenuated along the path from the source to the receiver [e.g. *Gorbatov et al.*, 2013]. The cumulative effect (denoted by S in Figure 1c) is an inherent characteristic of teleseismic signals, which show relatively high power in the lower end of the frequency spectrum. Consequently, this term modulates the appearance of the simple-looking autocorrelogram of an impulsive source drastically (Figure 1c) because the source autocorrelation is convolved with the autocorrelation of the impulse response. In general, the presence of the unknown time-dependent term would be a fundamental challenge in autocorrelation technique applications in high-resolution seismic imaging. In our particular case, we image a relatively short wavelength ice layer, and we attempt to address the above issue by balancing out the contribution of all frequency components.

Here, we present our scheme for data selection and processing to recover the high-frequency ice-base reflection from the recorded seismograms. Then we show an application to a station in Antarctica to demonstrate the technique's feasibility. Finally, a numerical simulation is shown to confirm our interpretation of real data.

METHODOLOGY

Data selection and quality assurance. To demonstrate the method, we use seismic data recorded at station ST01, deployed in the period from 2010 to 2012 in West Antarctica as a part of POLENET-ANET seismic network [*Chaput et al.*, 2014]. Seismogram segments of 30 s, from 10 s before the predicted arrival time by the *ak135* Earth model [*Kennett et al.*, 1995], are extracted from earthquake records with Mw $\geq$ 5.5 in epicentral distance range 30° - 95°. Next, by visual inspection, we discard the records containing clear instrument error, *pP* phase contamination, and those with poor signal to noise ratio. Subsequently, the selected segments are resampled to 40 samples per second and corrected for instrument response, and horizontal components are rotated to the radial transverse coordinate system.

Data processing. To obtain a single autocorrelogram for each event, we first apply frequency whitening (balancing) with an averaging window width of 0.5 Hz to balance the influence of all frequency components [*Bensen et al.*, 2007]. The whitened traces are then lowpass-filtered with a corner frequency of 5 Hz to mitigate the effect of very high-frequency noise also being amplified as a side-effect of the whitening operation. Because of the symmetry in the time response, we take only one-side of the autocorrelogram and taper its first 0.5 s using a cosine function to suppress the characteristic peak at time 0. To resolve finer resolution, we next filter the tapered trace with a 1 Hz high-pass filter.

Subsequently, we apply the phase-weighted stacking technique (PWS) of second order [*Schimmel and Paulssen*, 1997] to obtain a final stacked autocorrelogram that is clean and easy to interpret. The stacking method relies on the intrinsic coherence among all traces being stacked to suppress incoherent noise more efficiently and enhance reflection signals.

RESULTS

Figure 2a and 2b show vertical and radial one-sided autocorrelograms of seismograms recorded at station ST01. We plot individual autocorrelograms by their epicentral distance on the left panels and the stacked one on the right panels. In the left, characteristic negative phases are coherent on most vertical traces at around 1.5 s and radial ones at around 3.0 s, which add up to form prominent peaks on the right. Other peaks cancel out destructively. We interpret the prominent peaks as the first P and S reflection responses (2p and 2s), respectively. It is interesting to note that, because we use waveforms before the primary S phase arrival, the reflection on the radial component is purely due to the P-to-S converted energy at the ice-rock interface due to the off-vertical arrivals. Furthermore, the double reflection responses ($2p^2$ and $2s^2$), having a characteristic positive polarity and a double offset with respect to the first one, can also be clearly identified on both stacked autocorrelograms despite the fact that it is difficult to recognise them in the individual plots.

For the sake of simplicity, we eliminate the dependence on the ray parameter p in (1) by setting it to 0, because p ranging from 0.04 to 0.08 s/km (equivalent to the distance range from 30 to 95°) is relatively small in comparison with the other term (i.e. $1/v_p$ or $1/v_s$). This is confirmed by a visual inspection of the individual plots in Figure 1, where we can see that the first reflection negative peaks align almost perfectly on a horizontal line. First, we roughly estimate v_p/v_s ratio to be $\Delta t_s/\Delta t_p \approx 2$, which agrees well with previous glaciological results [e.g. *Kohnen*, 1974]. Furthermore, we use $v_p \approx 3.9$ km/s [*Chaput et al.*, 2014] as a reference value for the ice P wave velocity. Consequently, the ice thickness below station ST01 is estimated to be around 2.925 km, which is close to 2.943 km reported in Bedmap2 [*Fretwell et al.*, 2013].

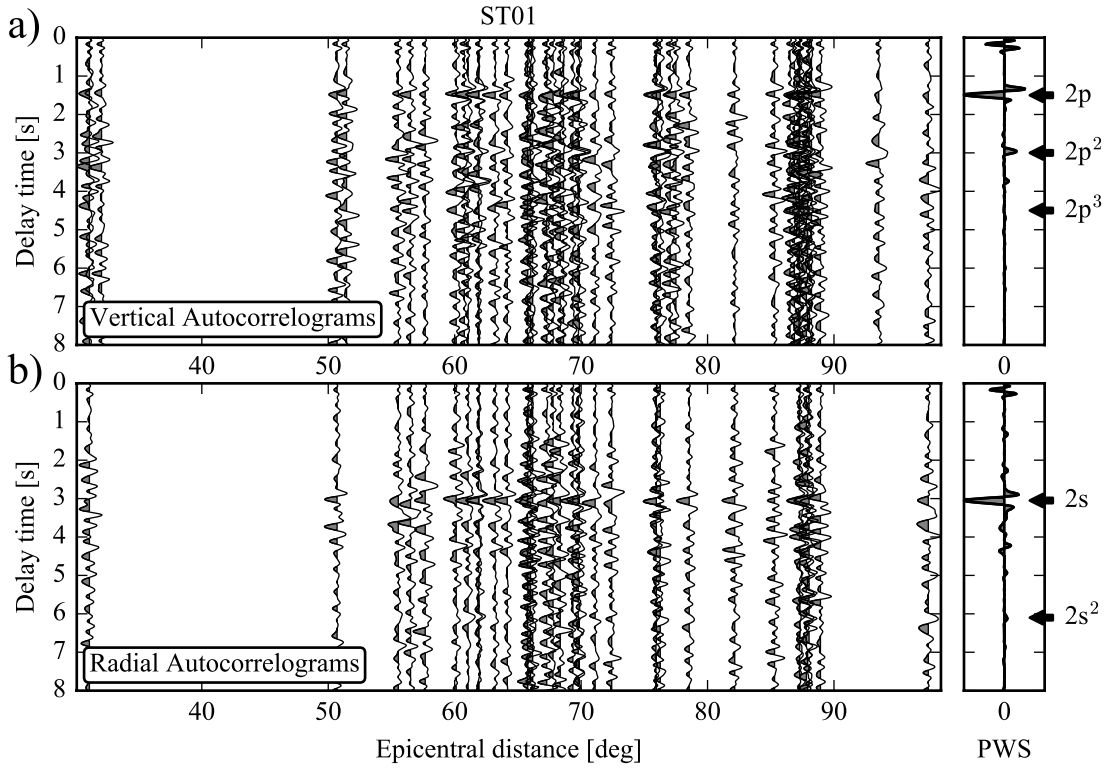

Figure 2 (a) Left: Autocorrelograms of vertical seismograms recorded at the Antarctic station ST01 plotted against epicentral distance; Right: Vertical stacked autocorrelograms with phase weighted stacking of order 2. (b) Same as (a) for radial component records.

In the following section, we present a synthetic experiment to test our ability to recover reflections from the ice-rock interface for the simple model in Figure 1a.

NUMERICAL SIMULATION

	v_p (km/s)	v_p/v_s	ρ (g/cm^3)
Ice	3.9	2.0	0.9
Rock	5.8	1.73	2.72

Table 1 Synthetic test input model.

Complete synthetic seismograms of distant events are generated by a two-step scheme. Table 1 summarises the Earth model parameters employed. First, to generate impulse response of the local structure, we use the synthetic seismogram algorithm by G. Randall (*respknt*), based on the method that was developed by *Kennett* (1983). Epicentral distance is converted to a ray parameter, which is used as an input to the algorithm. We can thus simulate the distance distribution of real earthquakes. Second, we generate a random function to synthetise the effect of source and travelling wave effects. To do so, we generate a trace of normally distributed random numbers. This trace is lowpass-filtered by a second order Butterworth filter to feature the characteristic low-frequency of seismic sources, and is tapered at both ends. The final synthetic seismogram is the convolution of the impulse response and the synthetised trace of the source response. This scheme is repeated to simulate the distribution of real earthquakes. We process synthetic seismograms in the same manner as the waveform data.

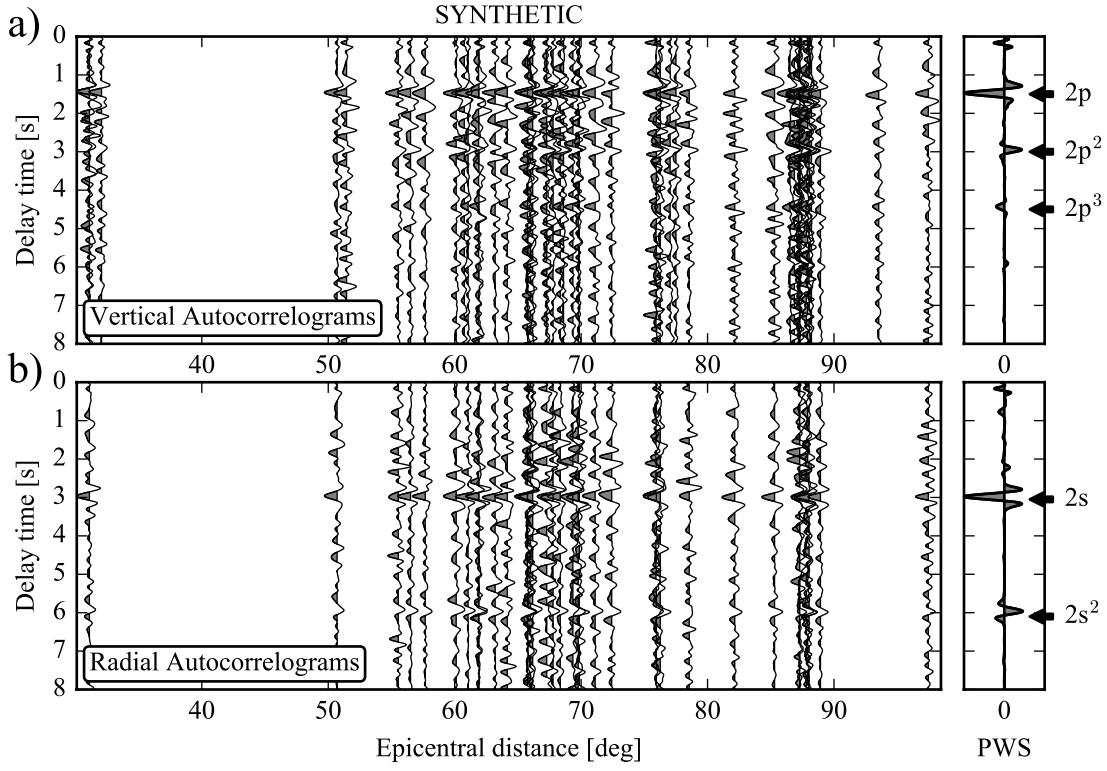

Figure 3 A synthetic experiment emulating the results shown in Figure 2. Synthetic events locations correspond to the real events locations. Epicentral distance is converted into ray parameters in numerical simulations.

Examples of synthetic autocorrelograms are shown in the lower two panels of Figure 1c. Figure 3 shows the same results as Figure 2 but for autocorrelograms of synthetic seismograms. Synthetic results appear to be similar to the real ones. They confirm the

emergence of reflection responses and their multiples on both components. The test also justifies our elimination of the dependence of the ray parameter p in interpreting the reflection signal. In this ideal case, more reflection responses can be seen due to the fact that both the simulated ice-rock interface and the wavefront are perfectly horizontal.

DISCUSSION AND CONCLUSION

The primary purpose of this study is to demonstrate the feasibility of a novel method for imaging a short wavelength structure such as the Antarctic ice layer, whilst addressing the problem of dominant low-frequency from seismic sources. Because the ice cap is reasonably well studied, it represents a good test case for our method. We expect to apply this technique in future to a region with a soft sediment layer overlying a hard basement.

We also want to promote the utilisation of the teleseismic P coda as an alternative method to interferometry studies focusing on long continuous records of ambient noise or the whole coda of an earthquake. First, it relies on a well-defined conceptual model as in the receiver function technique [*Langston*, 1979]. Second, although the pre-processing of data requires substantial effort, we have a better control on the quality of the data. Moreover, computations needed to produce the final results are much less demanding. On a negative side, the use of a relatively short P-wave coda segment in principle restricts the ability to resolve deep structures, from which the reflection times are longer.

In future studies, we plan to improve the autocorrelation technique by including constraints made on the ice cover, and incorporating such corrections make further inferences on the deeper structures such as the Moho discontinuity.

In conclusion, we have demonstrated the feasibility of using the stacked autocorrelation of teleseismic P coda in recovering reflection signals from the ice-rock interface in Antarctica by using data from a pilot station, ST01. The challenge of treating the low frequency characteristic of teleseismic signals is approached by using a frequency whitening operation. Next, by using both vertical and radial seismograms to produce stacked autocorrelograms, we observed not only P wave reflectivity, which is typically reported in previous autocorrelation studies, but also the emergence of strong S wave reflectivity. The ice thickness and v_p/v_s ratio of ice are then estimated from the picked reflection times.

REFERENCES

Bensen, G. D., M. H. Ritzwoller, M. P. Barmin, A. L. Levshin, F. Lin, M. P. Moschetti, N. M. Shapiro, and Y. Yang (2007), Processing seismic ambient noise data to obtain reliable broad-band surface wave dispersion measurements, *Geophys. J. Int.*, *169*(3), 1239–1260, doi:10.1111/j.1365-246X.2007.03374.x.

Chaput, J., R. C. Aster, A. Huerta, X. Sun, A. Lloyd, D. Wiens, A. Nyblade, S. Anandakrishnan, J. P. Winberry, and T. Wilson (2014), The crustal thickness of West Antarctica, *J. Geophys. Res. Solid Earth*, *119*(1), 378–395, doi:10.1002/2013JB010642.

Fretwell, P. et al. (2013), Bedmap2: improved ice bed, surface and thickness datasets for Antarctica, *The Cryosphere*, *7*(1), 375–393, doi:10.5194/tc-7-375-2013.

Gorbatov, A., E. Saygin, and B. L. N. Kennett (2013), Crustal properties from seismic station autocorrelograms, *Geophys. J. Int.*, *192*(2), 861–870, doi:10.1093/gji/ggs064.

Hansen, S. E., A. A. Nyblade, D. S. Heeszel, D. A. Wiens, P. Shore, and M. Kanao (2010), Crustal structure of the Gamburtsev Mountains, East Antarctica, from S-wave receiver functions and Rayleigh wave phase velocities, *Earth Planet. Sci. Lett.*, *300*(3–4), 395–401, doi:10.1016/j.epsl.2010.10.022.

Kennett, B. L. N. (1983), *Seismic Wave Propagation in Stratified Media*, Cambridge University Press.

Kennett, B. L. N., E. R. Engdahl, and R. Buland (1995), Constraints on seismic velocities in the Earth from traveltimes, *Geophys. J. Int.*, *122*(1), 108–124, doi:10.1111/j.1365-246X.1995.tb03540.x.

Kohnen, H. (1974), The temperature dependence of seismic waves in ice, *J. Glaciol.*, *13*(67), 144–147.

Langston, C. A. (1979), Structure under Mount Rainier, Washington, inferred from teleseismic body waves, *J. Geophys. Res. Solid Earth*, *84*(B9), 4749–4762, doi:10.1029/JB084iB09p04749.

Lythe, M. B., D. G. Vaughan, and the BEDMAP Consortium (2001), BEDMAP: A new ice thickness and subglacial topographic model of Antarctica, *J. Geophys. Res. Solid Earth*, *106*(B6), 11335–11351, doi:10.1029/2000JB900449.

Rondenay, S. (2009), Upper Mantle Imaging with Array Recordings of Converted and Scattered Teleseismic Waves, *Surv. Geophys.*, *30*(4–5), 377–405, doi:10.1007/s10712-009-9071-5.

Ruigrok, E., and K. Wapenaar (2012), Global-phase seismic interferometry unveils P-wave reflectivity below the Himalayas and Tibet, *Geophys. Res. Lett.*, *39*(11), L11303, doi:10.1029/2012GL051672.

Schimmel, M., and H. Paulssen (1997), Noise reduction and detection of weak, coherent signals through phase-weighted stacks, *Geophys. J. Int.*, *130*(2), 497–505, doi:10.1111/j.1365-246X.1997.tb05664.x.

Sun, W., and B. L. N. Kennett (2016), Receiver structure from teleseisms: Autocorrelation and cross correlation, *Geophys. Res. Lett.*, 2016GL069564, doi:10.1002/2016GL069564.

Zhu, L., and H. Kanamori (2000), Moho depth variation in southern California from teleseismic receiver functions, *J. Geophys. Res. Solid Earth*, *105*(B2), 2969–2980, doi:10.1029/1999JB900322.